JMEPEG (2012) 21:1008–1024
DOI: 10.1007/s11665-011-9951-y

1059-9495/$19.00

A Comparison of Fatigue Properties of Austempered Versus Quenched and Tempered 4340 Steel

John M. Tartaglia and Kathy L. Hayrynen

(Submitted January 4, 2011)

This study was conducted to determine if austempered 4340 steel had different fatigue resistance compared to quench and tempered (Q&T) 4340 steel with an identical hardness of nominally 45 HRC and an identical yield strength of nominally 1340 MPa (194 ksi). Strain-life and stress-life fatigue testing was conducted at room temperature under identical test conditions. The standard array of strain-life and stress-life regression constants was obtained. The two heat treatments produced virtually identical total strain-life curves and fatigue limits at 5 million cycles. However, the two materials exhibited different trends in the elastic and plastic strain regimes. The austempered steel exhibited greater high cycle fatigue (finite) lives than the Q&T samples at comparable elastic strain amplitudes in strain-life fatigue testing and at comparable stress amplitudes in stress-life fatigue testing. However, the Q&T samples exhibited greater low cycle fatigue lives than the austempered samples at comparable plastic strain amplitudes in strain-life testing. Although both materials generally exhibited similar fatigue fracture characteristics, the overload regions of the Q&T samples were composed entirely of dimple rupture, whereas the austempered samples exhibited both dimple rupture and quasicleavage.

Keywords Austemper, bainite, carbon/alloy steels, martensite, quench and temper, strain-life fatigue, stress-life fatigue

1. Introduction

1.1 Practical Significance, Property Variations, and Heat Treatment Differences

Quenched and tempered (Q&T) processing of medium carbon steels is the most common form of hardening and strengthening heat treatment. As a result, many researchers have extensively characterized the common properties and problems of Q&T steels, e.g., environmental embrittlement susceptibility under certain conditions.

Usage of austempered steels is less common, but they offer advantages over Q&T steels in some applications that require limiting distortion and residual stress (Ref 1). An early study (Ref 2) also showed that austempered steels with lower bainite microstructures offer improved Charpy impact toughness versus their Q&T counterparts with predominantly martensitic microstructures.

In a recent investigation (Ref 3), the present authors conducted a study to determine if austempered 4340 steel had different toughness and hydrogen embrittlement resistance when compared to quench and tempered (Q&T) 4340 steel with an identical yield strength of 1340 MPa (194 ksi). Baseline comparison showed that the austempered steel with a lower bainite microstructure exhibited higher hardness, tensile strengths, Charpy V-notch (CVN) impact toughness and ductility at both low −40 °C (−40°F) and ambient temperatures as compared to the Q&T steel with a martensite microstructure. After machining and just prior to testing, subsize CVN specimens and notched bend specimens were immersed in hydrochloric acid-water baths. Hydrogen embrittlement resistance was higher for the austempered steel as compared to the Q&T steel. No differences in room temperature CVN energy resulted from hydrogen charging of the austempered and Q&T steel versus their unexposed counterparts. However, in the notched bend specimens, the hydrogen charging caused significant peak load decreases (40%) for the Q&T steel, while the austempered steel exhibited only small (6%) decreases in peak load. Intergranular cleavage fracture occurred solely in the charged Q&T bend samples, which is further evidence of their embrittlement.

The differences between the martensitic and the lower bainite microstructures of Q&T and austempered steels, respectively, are thoroughly reviewed in Ref 3. However, the two microstructures are briefly summarized here. Bainite forms by the decomposition of austenite to acicular ferrite and carbides at a temperature above the martensite-start (Ms) temperature. The two primary forms of bainite are upper bainite and lower bainite. In upper bainite, the carbides are typically located between the acicular ferrite grains; however, in lower bainite, the carbides tend to precipitate at an inclined angle to the major growth direction or longitudinal axis of the acicular ferrite grains (Ref 4).

A partial or fully bainitic microstructure can form by continuous cooling (slack quenching). This type of bainite usually forms inadvertently during Q&T treatments intended to form all martensite, due to insufficient alloy content, oversize sections, or insufficient quench speed. This Q&T process results in a microstructure containing all bainite or some bainite

John M. Tartaglia, Engineering, Stork Climax Research Services, Wixom, MI; and **Kathy L. Hayrynen**, Technical Division, Applied Process Inc, Livonia, MI. Contact e-mail: John.tartaglia@us.stork.com.

interspersed within a martensitic matrix. A final mixed microstructure results when bainite forms by continuous cooling or slack quenching.

Because the bainite transformation by continuous cooling occurs over a range of temperatures, its microstructural refinement is inconsistent. As a result, bainite formed by continuous cooling is usually considered undesirable.

Austempering utilizes a quench temperature above the Ms temperature with an isothermal transformation time sufficient to exceed the bainite-finish time. When bainite forms by isothermal transformation or austempering, the resulting microstructure is uniform and refined as compared to bainite that forms during continuous cooling. Steels with high alloy contents may contain a small percentage of martensite in the final microstructure. However, this microstructure is not like a slack quench microstructure where the predominant matrix microconstituent is martensite rather than bainite.

1.2 Literature Review of Heat Treatment Effects on Fatigue Resistance

A literature search revealed numerous references regarding heat treatment effects on the fatigue behavior of hardened steel. Various studies compared the fatigue properties obtained with differing microstructures, but no single conclusion about the best microstructure for fatigue resistance was available. In fact, selected papers stated opposite conclusions about which heat treatments and microstructures were better for enhancing fatigue resistance, especially when different fatigue testing protocols were evaluated, as discussed in this section of this article.

In a fatigue crack propagation study (Ref 5) of 4340, increasing volume fractions of a ductile second phase increased the fatigue resistance. Furthermore, when the second phase was highly tempered martensite, the authors found better fatigue crack growth resistance than when the second phase was lower bainite.

Another set of authors compared (Ref 6) the bending fatigue properties of conventional and modified austempering, to quench and tempered 0.6 wt.%C-0.5S-0.8 Mn steel. The modified austempering treatment consisted of austenitizing at 860 °C, interrupted quenching to 260 °C, austempering at 400 °C, water quenching, and 200 °C tempering. The modified austempered steel has a triple phase structure consisting of carbide-free upper bainite, 26 vol.% austenite and 10 vol.% martensite. This modified austempered steel had a higher bending fatigue limit than conventionally austempered steel and significantly decreased fatigue factor versus the quench and tempered steel. However, the modified austempered steel had a similar fatigue limit to the quenched and tempered steel.

Other investigators have found that austempered steels have higher fatigue strength (Ref 7), lower fatigue crack propagation rates (Ref 7-9), and lower fatigue threshold stress intensity (Ref 9) than martensitic steels in 0.45C-1.5Cr-1.5Si-0.1V steel (Ref 7), medium carbon trip steel (Ref 8), and LM2 steel (Ref 9). Conversely, other authors found that the fatigue strength of martensitic steels was higher than that of austempered medium alloyed structural steels (UNI40 NiCrMo7, 42NCD4, 35NCD4, and 30CD12) (Ref 10) and low carbon-low alloy 8620 steel (Ref 11). However, the same authors (Ref 11) did find that the strength and threshold stress intensity of the austempered steel and a duplex ferrite-martensite steel were greater than those of hot-rolled ferrite-pearlite steel.

Some authors have investigated the fatigue properties of 0.2%C steels with various Q&T heat treatment variations. One (Ref 12) of the present authors examined the effects of martensite content, obtained by forming varying portions of bainite formed by continuous cooling and slack quenching of 8622 and 8822 steels. When fatigue test results were compared at a tensile strength of 1240 MPa (180 ksi), impact toughness, actual and predicted fatigue lives in the high cycle regime increased with martensite content, but low cycle fatigue resistance was relatively unaffected. Fatigue strength and ultimate tensile strength were directly related, and all the quenched and tempered steels exhibited cyclic softening.

In addition to the modified austempering mentioned above (Ref 6), other authors have studied modified and combination Q&T and austempering heat treatments. One author (Ref 13) evaluated the four-point bending fatigue properties of a 20CrMnMo steel with a combination of low carbon martensite and bainite formed by oil quenching and austempering at 360 °C. The formation of 20% lower bainite remarkably increased the threshold stress intensity and lowered crack propagation rates. Another set of authors (Ref 14) evaluated isothermal austempering versus successive austempering and modified up-quenching austempering heat treatment. The latter combination produced the best combination of strength and ductility, but the authors did not evaluate fatigue properties.

1.3 Purpose of this Study

Low cycle fatigue (LCF) testing (performed in strain control) of quenched and tempered low alloy steels such as 4340 has been conducted extensively (Ref 15-17). Furthermore, some fatigue data have been obtained on austempered 1060 and 5150 steels (Ref 17). LCF properties (Ref 15, 17) and crack propagation rates (Ref 18) have been studied extensively as a function of monotonic strength (Ref 17, 18) and tempering temperature.

However, the present investigators found only one article (Ref 10) that compared high cycle fatigue properties of austempered and Q&T steels at the same monotonic property levels. It is important to perform such fatigue property comparisons while keeping one or more of the monotonic properties (yield strength, tensile strength, or elongation) constant. Most heat treatments can produce a wide range of monotonic properties depending on the selected heat treatment parameters, e.g., tempering temperature, and the fatigue properties may vary similarly, so it is important to keep at least one parameter constant in any comparison.

The present authors showed that austempered 4340 steel had higher yield strength, impact toughness, and hydrogen embrittlement resistance versus Q&T 4340 steel in the earlier study (Ref 3), and we recommended that fatigue properties be similarly assessed. Following those recommendations, the authors designed this study to evaluate the fatigue properties obtained with the same two heat treatment conditions. The austempering and Q&T heat treatments were evaluated with the same monotonic strength to assess whether they produced differences in both low cycle (strain controlled) and high cycle (stress-controlled) fatigue testing. This study seems unique and could be a worthwhile property compendium to common fatigue databases (Ref 15, 18). This study also includes a systematic evaluation of the fractographic characteristics of austempered versus Q&T 4340 steel.

2. Experimental Procedures

2.1 Work Scope

To properly compare fatigue resistance for austempered versus Q&T processing, the first requirement is that the same steel composition must be subjected to the two heat treatments. The present investigators chose SAE 4340 steel (UNS G43400) steel because it is a common medium carbon steel.

Secondly, the steel must also be heat-treated to the same hardness where Q&T processing can result in differing fatigue properties. In the previous study (Ref 3), the authors chose 45 HRC to both comply with common hydrogen embrittlement susceptibility and generate useful data for commonly specified 4340 applications, the authors targeted 45 HRC for this study.

In the previous study (Ref 3), the authors verified that the properties of the austempered and Q&T samples typified the steel and respective heat treatment. The composition, hardness, tensile properties, and Charpy impact toughness at room and low temperature were measured. Continuing to use the same steel and heat treatment conditions for this study had the auxiliary benefit that the investigators obtained useful microstructural, monotonic mechanical property, and fractographic engineering data for design and failure analysis.

2.2 Materials and Their Characterization

The investigators were supplied with UNS G43400 steel bar samples that were nominally 25 mm (1 in.) in diameter by 125 mm (5 in.) in length. The bars were commercially heat treated by austenitizing at 885 K (1625°F) and either quenching in oil at 71 K (160°F), followed by tempering, or austempering at 312 K (594°F) to a desired hardness of nominally 45 Rockwell C.

Two sets of bars were supplied and heat treated in two batches for the purposes of this study. The first batch was used for the prior study and the strain-life fatigue testing and fractography conducted in this study. The second batch of bars was used for the stress-life fatigue and staircase fatigue testing in this study.

Elemental contents of one sample from each steel batch were determined using glow discharge-optical emission spectrometry (GD-OES) in general accordance with ISO standard 14707 (Ref 19) except for carbon, sulfur, and nitrogen, which were determined using combustometric methods (LECO) in accordance with ASTM standard E1019 (Ref 20).

Sections were cut from Q&T bars and austempered bars of both batches and Rockwell hardness measurements were made on the transverse cross sections in accordance with ASTM standard E18 (Ref 21).

Transverse and longitudinal sections were cut from a Q&T bar and an austempered bar from Batch 1. The sections were mounted and polished using standard metallographic techniques for low alloy steel in accordance with ASTM standard E3 (Ref 22). Optical micrographs were taken after etching in 10% sodium metabisulfite. Inclusion content cleanliness measurements were also determined, but these were exclusively reported earlier (Ref 3).

2.3 Monotonic Mechanical Testing

Three tensile specimens were machined from both the austempered and the Q&T steels. The tensile specimens had threaded grip ends and gauge diameters of 9 mm (0.35 in.) and lengths of 36 mm (1.4 in.).

For each heat treatment condition in both batches, duplicate tensile tests were conducted with an extensometer and strain gauge at room temperature to determine 0.2% offset yield strength (YS), ultimate tensile strength (UTS), and total elongation (El) in accordance with ASTM standard E8 (Ref 23). In composition and heat treatment Batch 1, elastic modulus (E) was determined in accordance with ASTM standard E111 (Ref 24) and monotonic strength coefficient (K) and strain hardening exponent (n) were determined in accordance with ASTM standard E646 (Ref 25).

For all tensile tests, the samples were tested at strain rates of 0.3%/min and 10%/min in the elastic and plastic ranges, respectively. The percent elongation at fracture was determined using the total elongation measured by the extensometer.

The low temperature tensile and impact properties were determined and exclusively reported earlier (Ref 3).

2.4 Strain-Life Fatigue Testing

Strain-life fatigue specimens were prepared in accordance with the ASTM standard E606 (Ref 26) recommendations for sample geometry and machining practice for the austempering and Q&T heat treatments that resulted in the similar ultimate strengths. The cylindrical specimens possessed uniform gauge sections that were 16 mm (0.63 in.) in length and 8 mm (0.315 in.) in diameter. The specimens were prepared such that no heating of the gauge sections occurred, and the gauge sections were polished by machine to a glossy finish with no cylindrical scratches in the gauge section. Further specimen details are shown in Fig. 1.

Fully reversed strain-life fatigue tests were performed at room temperature on a servohydraulic fatigue machine in accordance with ASTM standard E606 (Ref 26). After partially randomizing, ten (10) samples of the Q&T and eleven (11) samples of the austempered condition were tested. A longitudinal extensometer was mounted on each specimen. The tests were performed in strain control, under control of a fully reversed ($R = -1$) total strain cycle with a triangular waveform and a constant strain rate of 2%/s. The gauge length of the extensometer was 8 mm (0.3 in.). The saturation stress ($\Delta\sigma/2$) and actual plastic strain ($\Delta\varepsilon_p/2$) amplitudes were measured at half-life, i.e., one-half the number of cycles to failure (N_f) defined as specimen fracture. The modulus of elasticity (E) of each material was obtained from the tensile testing.

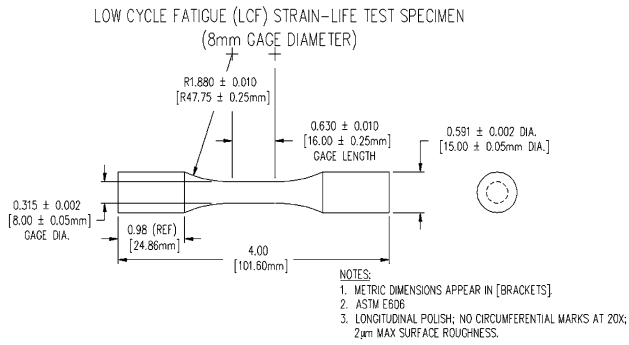

Fig. 1 Schematic of strain-life fatigue sample

For low applied total strain amplitudes, fatigue tests were performed in strain control well past saturation, i.e., when the load amplitude remained constant, and when 100,000 cycles were reached. To minimize machine time, these low strain tests were then continued in load control using the last maximum and minimum loads achieved in strain cycling, and a 30-Hz sinusoidal waveform until failure or survival was reached. Failure was defined as two-piece separation, or until a 20% drop in stress range occurred. Test survival (runout) was defined as 5 million cycles. All samples were tested at single strain amplitudes and duplicate samples were tested at selected strain amplitudes.

The plastic strain amplitude ($\Delta\varepsilon_p/2$) and fatigue reversal regression constants (σ_f', b, ε_f', and c) were determined using the procedures outlined in ASTM standard E606 (Ref 26) and the appendix of this article. For both materials, the cyclic strength coefficient (K') and cyclic strain hardening exponent (n') were calculated (see appendix) using the fatigue-reversal regression constants obtained from the strain-life tests.

2.5 Stress-Life and Staircase Fatigue Testing

Stress-life fatigue specimens were prepared in accordance with the ASTM standard E466 (Ref 27) recommendations for sample geometry and machining practice for the austempering and Q&T heat treatments that resulted in the similar ultimate strengths. The cylindrical specimens possessed uniform gauge sections that were identical to the strain-life fatigue samples, i.e., 16 mm (0.63 in.) in length and 8 mm (0.315 in.) in diameter. The specimens were prepared such that no heating of the gauge sections occurred, and the gauge sections were polished by machine to a glossy finish with no cylindrical scratches in the gauge section. Further specimen details are shown in Fig. 2; note that the blend radii dimension was slightly different than that shown in Fig. 1 for the strain-life sample, but this is consistent with the different recommendations in ASTM standards E466 (Ref 27) and E606 (Ref 26).

Fully reversed stress-life fatigue tests were performed at room temperature on a servohydraulic fatigue machine in accordance with ASTM standard E466 (Ref 27). After randomizing, ten (10) samples of the Q&T and ten (10) samples of the austempered condition were tested. The tests were performed in load control, under control of a fully reversed ($R = -1$) total stress cycle with a sinusoidal waveform and a constant frequency of 32.5 Hz. Load was monitored throughout each test and failure was defined as two-piece separation. Test survival (runout) was defined as 5 million cycles. All samples were tested at single stress amplitudes.

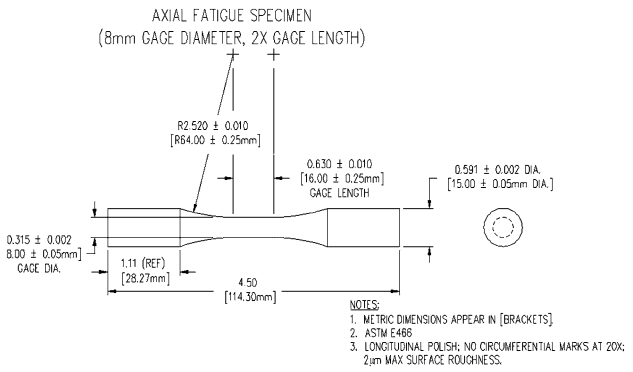

Fig. 2 Schematic of stress-life fatigue sample

Fatigue limit (or the fatigue strength at 5 million cycles), per ASTM standard E1820 (Ref 28), was determined using a staircase testing protocol. This protocol was originally developed (Ref 29) to evaluate drug toxicity. The staircase or up-and-down protocol was modified to become a common ASTM standard E739 (Ref 30) fatigue testing program used to determine the median fatigue limit (Ref 31). Further extensions of the protocol testing and analysis produce a mean fatigue limit with a standard (Ref 32), as commonly employed for cast metals with General Motors worldwide standard GMN7152 (Ref 33).

Staircase testing programs start by testing the first specimen at a stress near the estimated fatigue limit. The remaining specimens are tested sequentially, increasing the applied stress for the next specimen if the previous specimen survives or decreasing the stress for the next specimen if the previous specimen fails. An initial stress amplitude of 724 MPa (105 ksi) and step size of 34 MPa (5 ksi) were employed as the staircase testing parameters for this study.

2.6 Fractography

To characterize the fracture mode of the strain-life fatigue specimens, all fracture surfaces were examined by naked eye and an optical stereoscope. Selected sample fracture surfaces were documented and examined with an optical stereo microscope and scanning electron microscope (SEM). The SEM was operated with 20 kV accelerating voltage and in secondary electron (SE) mode. The pictures were taken at selected magnifications and depths below the smooth strain-life specimens to facilitate fractographic comparison between the heat treatments conditions. Three strain level and samples were selected for the optical and SEM fractographic documentation of the austempered samples, and two of these were selected for the Q&T samples.

3. Results

3.1 Composition and Microstructure

The results of the chemical analyses of Q&T and austempered samples are shown in Table 1. Both samples tested conformed to the chemical specifications for SAE 4340 and UNS G43400 low alloy steel contained in SAE standard J404 (Ref 34) and AMS-6415 (Ref 35).

Composition Batch 1 was employed for the strain-life fatigue samples and Composition Batch 2 was employed for the stress-life fatigue samples. The two batches were reasonably similar in composition to be considered identical in terms of how they would affect metallurgical characteristics and mechanical properties.

Figures 3 to 6 are optical micrographs of the mounted specimens after they were etched in 10% sodium metabisulfite. All the micrographs were obtained in the interior of the bar at an original magnification of 500×. Etching with sodium metabisulfite helps identify the difference between martensitic and bainitic microstructures because martensite appears straw brown and bainite appears blue.

Figure 3 shows that the Q&T samples typify a tempered martensite structure and Fig. 4 shows that the austempered

Table 1 Chemical analysis of 4340 steel samples (in wt.%)

Batch	1		2			
Condition	Austempered	Q&T	Annealed		4340 specifications	
Data source	Stork CRS		Steel supplier		AMS-6415	SAE J 404
C	0.42	0.40	0.41	0.40	0.38-0.43	0.38-0.43
S	0.019	0.019	0.02	0.015	0.025 max.	0.040 max.
P	0.010	0.010	0.01	0.008	0.025 max.	0.030 max.
SI	0.24	0.24	0.26	0.27	0.15-0.35	0.15-0.35
MN	0.75	0.76	0.73	0.75	0.65-0.85	0.60-0.80
CR	0.81	0.80	0.80	0.81	0.70-0.90	0.70-0.90
NI	1.79	1.80	1.66	1.66	1.65-2.00	1.65-2.00
MO	0.26	0.25	0.25	0.25	0.20-0.30	0.20-0.30
V	0.006	0.006	0.005	0.003	…	…
AL	0.023	0.023	0.024	0.026	…	…
CU	0.16	0.16	0.16	0.16	0.35 max.	0.35 max.
TI	<0.005	<0.005	…	…	…	…
CO	0.016	0.016	…	…	…	…
ZR	<0.005	<0.005	…	…	…	…
NB	<0.005	<0.005	0.001	0.001	…	…
TA	0.019	0.019	…	…	…	…
W	<0.01	<0.01	…	…	…	…
B	<0.0005	<0.0005	…	…	…	…
N	0.005	0.004	0.0041	0.0083	…	…

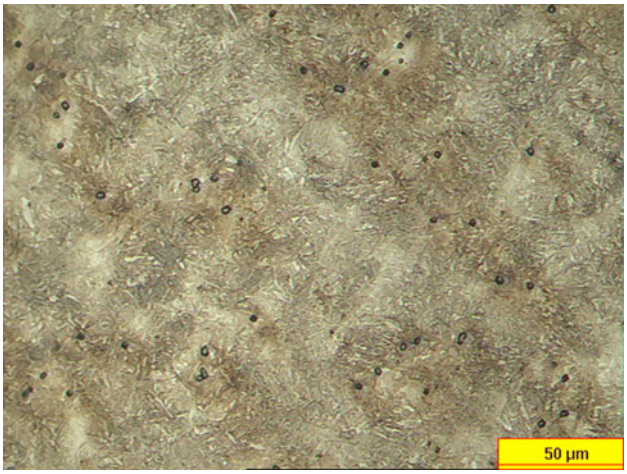

Fig. 3 Optical micrograph of transverse section of Q&T sample

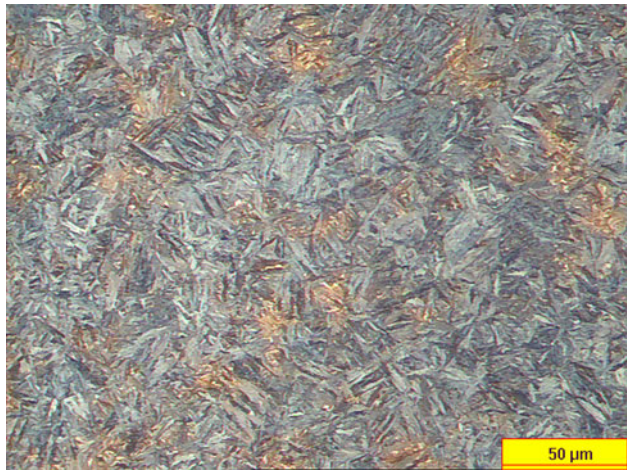

Fig. 4 Optical micrograph of transverse section of austempered sample

specimens are mostly bainitic with some untempered martensite. Figure 5 shows that the samples are heavily banded in the longitudinal orientation. The light etching regions are probably enriched with carbon and manganese, and they contain most of the manganese sulfide inclusions. Figure 6, which is the same condition as Fig. 3, but with a different sample, shows that the bands are actually tubular "packets" with highly alloyed boundaries.

3.2 Monotonic Mechanical Properties

The Rockwell C hardness (HRC) results are presented in Table 2, along with strength conversions from ASTM standard A370 (Ref 36). Each row in the table represents results obtained on a single sample. The rows in the table showing only average results were obtained by Applied Process; the rest of the hardness data were obtained by Stork CRS.

Both samples in composition and heat treatment Batch 1 conformed to the previously stated hardness requirement of approximately 45 HRC, with the austempered samples having slightly higher hardness. The hardness was relatively constant across the cross section and mechanical test specimens were only obtained from the central 19 mm (0.75 in.) of the bar (Ref 3).

The samples showed slightly greater scatter in the hardness data from composition and heat treatment Batch 2. Again, the data conformed to the 45 HRC hardness requirement within the standard industrial reproducibility in commercially cast, forged, and heat-treated product.

Table 3 shows the room temperature tensile test results for both heat treatment conditions. Each row in the table represents the results obtained on a single sample. Yielding behavior and low temperature test results were published earlier (Ref 3).

Some differences in tensile properties were observed between the batches, but the differences are considered insignificant. The tensile properties are considered similar to the extent that they are within the standard industrial reproducibility in commercially cast, forged, and heat-treated product. Furthermore, the tensile strengths of the austempered and Q&T samples were virtually identical with predictions based on hardness from ASTM standard A370, as shown in the last column of Table 2. Also, the differences in monotonic strength were considered to be sufficiently similar with respect to how they would affect both high and low cycle fatigue properties. Therefore, the authors made an affirmative decision after the strain-life fatigue testing of the Batch 1 samples to continue the stress-life testing of Batch 2 samples and to compare the results between the two batches as if there were no differences between the batches.

Fig. 5 Optical micrograph of longitudinal section of Q&T sample

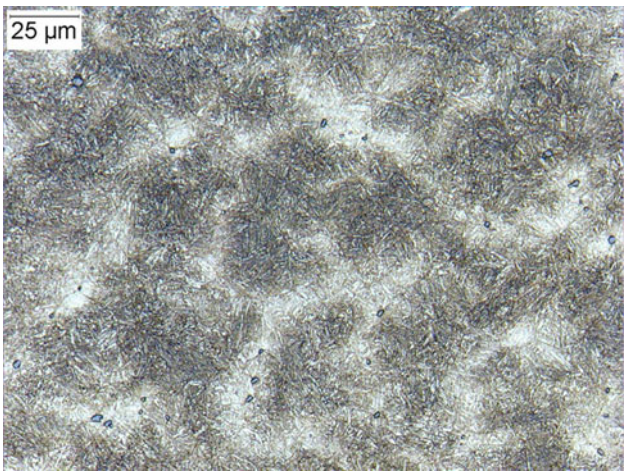

Fig. 6 Optical micrograph of a transverse section of a different Q&T sample than Fig. 3

3.3 Strain-Life (Low Cycle) Fatigue Properties

Table 4 contains a listing of the strain-life fatigue data for all the Batch 1 specimens corresponding to both heat treatment (austempered vs. Q&T) conditions. The total strain, plastic strain, and elastic strain amplitudes are plotted versus fatigue cycles in Fig. 7, 8, and 9, respectively. (Note that Table 4 contains plastic strain and stress range data, and the plots show strain amplitude data.) In almost all cases, the initial stress amplitude was greater than the saturation stress amplitude shown in Table 4; therefore, cyclic strain softening was obtained with both heat treatments.

Figures 7 to 9 also contain logarithmic linear strain regression lines calculated using the appendix, and the stress versus reversals and strain versus reversals regression constants in Table 5. Although Table 4 shows that one of the samples had a shoulder break, the results for this sample A21 were used in the regression analyses because their goodness-of-fits, as measured by the coefficient of determination (r^2) values, were unaffected.

Figure 7 shows that the two heat treatments had very similar fatigue lives at most total strain amplitudes. However, when the total strain amplitude is separated into its plastic and elastic components, Fig. 8 and 9 shows remarkable differences in behavior for the two heat treatments. Versus the Q&T samples, the austempered samples exhibit significantly higher lives at the same elastic strain amplitudes (see Fig. 8) and slightly lower lives at the same plastic strain amplitudes (see Fig. 9). The regression lines demonstrate these trends very well and the coefficients of determination values (see Table 5) are reasonably close to unity, considering the limited data sets. (The high

Table 2 Rockwell hardness results (HRC)

Batch	Condition	Measurement #							Average	Approximate UTS MPa (ksi)
		1	2	3	4	5	6	7		
1	Austempered	47.1	46.9	46.8	45.6	46.4	46.9	47.0	46.7	1580 (229)
	Q&T	44.6	44.5	43.8	44.7	44.1	44.9	44.7	44.5	1450 (210)
2	Austempered	46.5	46.9	47.5					47.0	1580 (229)
	Austempered	43.6	45.1	45.5					44.7	1480 (215)
	Austempered								45.5	1520 (221)
	Austempered								45.7	1520 (221)
	Q&T	46.1	44.6	44.3					45.0	1480 (215)
	Q&T	42.4	43.4	43.1					43.0	1390 (201)
	Q&T								44.5	1480 (215)
	Q&T								45.4	1480 (215)

Table 3 Tensile test results

Batch	Condition	Yield strength (0.2% offset) MPa (ksi)	Ultimate tensile strength MPa (ksi)	Elongation (a), %	Reduction of area, %	Elastic modulus GPa (Mpsi)	Monotonic strength coefficient (K) MPa (ksi)	Strain hardening exponent, n
1	Austempered	1340 (195)	1610 (233)	14.2	56.1	211 (30.6)	2250 (326)	0.087
		1340 (194)	1600 (232)	14.2	57.2	208 (30.2)	2240 (324)	0.087
	Q&T	1340 (195)	1470 (213)	12.7	50.1	210 (30.5)	1860 (270)	0.058
		1340 (195)	1460 (213)	12.9	50.8	210 (30.5)	1870 (272)	0.061
2	Austempered	1270 (184)	1520 (220)	14.4	57.0	…	…	…
		1270 (184)	1510 (219)	14.0	56.0	…	…	…
	Q&T	1320 (191)	1440 (209)	13.0	51.0	…	…	…
		1320 (191)	1440 (209)	13.0	49.0	…	…	…

(a) For Batch 1, elongation at fracture was determined by total elongation measured by extensometer; for Batch 2 elongation was determined by reassembly of samples

Table 4 Strain-life (low cycle) fatigue results (Batch 1)

Test order (for each heat treatment)	Condition and specimen ID (A = Austemper) Q = Q&T)	Frequency, Hz	Total strain amplitude, Δε/2, %	Stress range at half life, Δσ		Plastic strain range at half-life, $\Delta\varepsilon_p$, %	Cycles, N_f
				MPa	ksi		
1	A1	1	0.50	2042	296.2	0.017	22,886
2	A2	1	0.50	2036	295.3	0.014	12,275
3	A4	0.5	1.00	2517	365.1	0.715	772
4	A19	0.357	1.40	2717	394.1	1.433	189
5	A9	0.666	0.75	2372	344.1	0.300	2,073
6	A16	0.833	0.60	2250	326.3	0.086	6,954
7	A17	1.25	0.40	1642	238.1	0.010	72,017
8	A21	1.43	0.35	1441	209.1	0.008	429,013(a)
9	AU1	1.25	0.40	1637	237.4	0.012	162,044
10	AU2	0.416	1.20	2574	373.3	1.048	510
11	AU3	0.5	1.00	2563	371.8	0.700	517
1	Q9	1	0.50	1729	250.7	0.144	13,479
2	Q15	1	0.50	1729	250.7	0.143	12,408
3	Q19	0.357	1.00	2005	290.8	0.974	681
4	Q17	0.5	1.00	1963	284.7	0.991	1,029
5	Q18	0.416	1.20	2076	301.1	1.319	583
6	Q16	0.833	0.60	1750	253.8	0.321	6,575
7	Q20	1.25	0.40	1644	238.5	0.010	43,319
8	Q21	1.43	0.35	1471	213.4	0.008	294,680
9	QU1	0.666	0.75	1845	267.6	0.554	3,066
10	QU2	1.25	0.40	1645	238.6	0.010	53,503

(a) Shoulder break

r^2 value shows that the fractional portion of the total variance is explained well by the regression predictions versus the unexplained variance portion or regression model error.)

Eq 6 in the appendix was used to calculate the transition fatigue life N_t, which represents the life at which the elastic and plastic regression lines intersect (Ref 37). This is the life at which the stabilized hysteresis loop has equal elastic and plastic strain components. This is sometimes defined as the transition from low and high cycle fatigue in a material. The regression equations for both materials are plotted together in Fig. 10, without the data (which are shown in Fig. 7). Table 5 shows that the transition fatigue life was significantly different for the two heat treatments, with N_t values of 289 and 1313 cycles for the austempered and Q&T specimens.

3.4 Stress-Life (High Cycle) Fatigue Properties

The austempered samples exhibited significantly higher experimental fatigue lives (see Table 4) and predicted lives (see Fig. 9) at the same elastic strain amplitudes. Therefore, the high cycle fatigue properties were determined to assess whether this difference extended to the high cycle regime.

Table 6 contains a listing of the stress-life fatigue lives for all the Batch 1 specimens corresponding to both heat treatment (austempered vs. Q&T) conditions. Figures 11 and 12, respectively, shows semilogarithmic and logarithmic presentations of the stress-life fatigue data shown in both Table 4 and 6 for both Batch 1 and 2 specimens. (Note that Table 4 and 6 contains stress range data and the plots show stress amplitude data.)

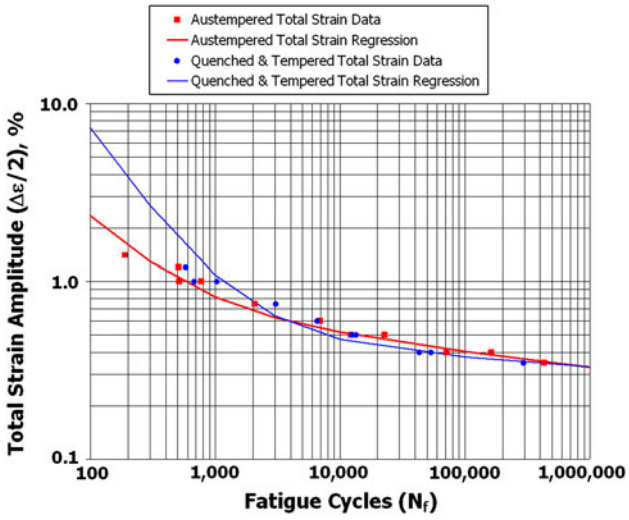

Fig. 7 Total strain amplitude versus fatigue life (for Batch 1)

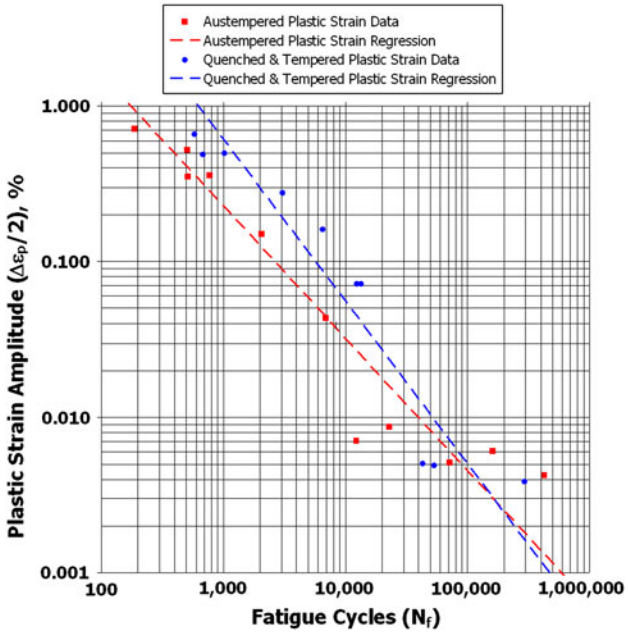

Fig. 8 Plastic strain amplitude versus fatigue life (for Batch 1)

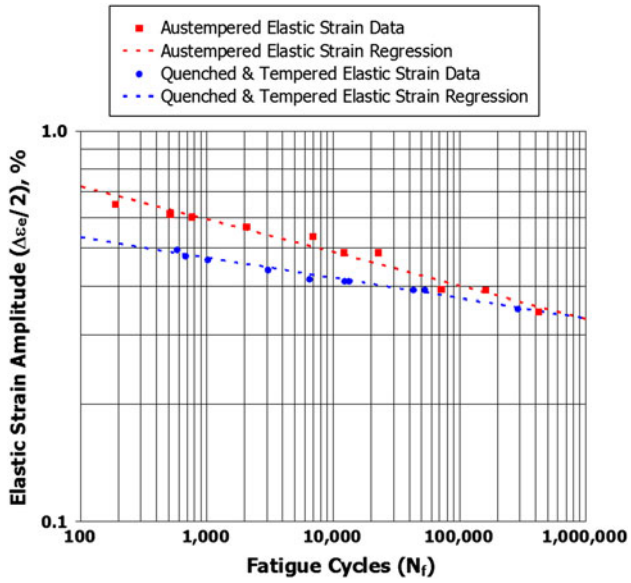

Fig. 9 Elastic strain amplitude versus fatigue life (for Batch 1)

Table 5 Cyclic strain versus reversals regression constants (Batch 1)

Regression constant or calculation	Austempered	Q&T	Units
Elastic modulus, E	209	211	GPa
	30.4	30.5	Mpsi
Fatigue strength(a)			
Coefficient, σ_f'	2340	1463	MPa
	339.3	212.2	ksi
Exponent, b	−0.0835	−0.0516	
Coefficient of determination, r^2	0.972	0.982	
Fatigue ductility(a)			
Coefficient, ε_f'	1.4669	16.959	
Exponent, c	−0.8503	−1.0422	
Coefficient of determination, r^2	0.911	0.910	
Transition life(b), N_t	289	1,317	Cycles

(a) Defining equation: $\Delta\varepsilon/2 = (\sigma_f'/E)\,(2N_f)^b + \varepsilon_f'\,(2N_f)^c$
(b) Defining equation: $N_t = 0.5\,(\varepsilon_f' E/\sigma_f')^{1/(b-c)}$

Figures 11 and 12 also contain, respectively, semilogarithmic and logarithmic linear stress regression lines calculated using the appendix, equations from ASTM standard E739 (Ref 30), and the constants shown in Table 7. Although Table 6 shows results for several samples that had shoulder breaks, the results for these samples were used in the regression analyses because their goodness-of-fits, as measured by the coefficient of determination (r^2) values, were unaffected.

Figures 11 and 12 show that the fatigue lives of the austempered samples are about 1 to 2 decades greater at high stresses as compared to the Q&T result. This difference diminishes rapidly with decreasing stress until the two curves essentially converge at 1 million cycles.

To be included in the mean fatigue limit calculation, the staircase protocol requires that samples either survive or fracture in the gauge section. Therefore, the shoulder fractures in Table 6 were ignored and another sample was tested at the same stress. Only a few samples met the gauge section fracture criterion, and Table 8 shows these selected results.

Figure 13 shows the staircase results in graphical form. Both austempered and Q&T samples had identical mean fatigue limit of 689 MPa (100 ksi) and standard deviation of 26 MPa (3.8 ksi) at 5 million cycles. This is consistent with the trends predicted from the plots of stress-life results in Fig. 11 and 12, where the fatigue strengths converged to about the same value at 1 million cycles.

3.5 Fractography

Tables 9 and 10 show respective summaries of the fractographic results for the austempered and Q&T strain-life fatigue samples. The columns corresponding to the five samples that were examined and documented with the stereoscope and SEM are indicated in red. All other samples were examined visually.

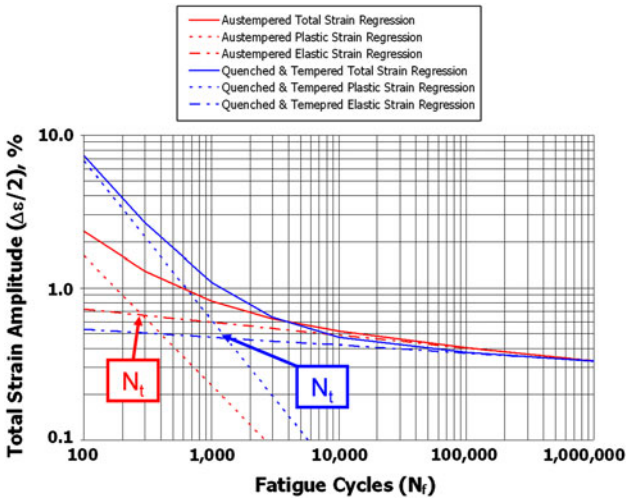

Fig. 10 Strain amplitude versus fatigue life regressions and calculated transition life (N_t)

Table 6 Stress-life (high cycle) fatigue results (Batch 2)

Test order (for each heat treatment)	Condition and Specimen ID (A = Austemper) Q = Q&T)	Stress range, Δσ		
		MPa	ksi	Cycles, N_f
12	AA12	1448	210	1,215,605
13	AA10	1379	200	5,000,000(b)
14	AA08	1448	210	561,065(a)
15	AA11	1448	210	409,571(a)
16	AA13	1448	210	672,218
17	AA06	1379	200	3,330,768
18	AA04	1310	190	5,000,000(b)
19	AA05	1379	200	567,098(a)
20	AA07	1379	200	818,666(a)
21	AA09	1310	190	5,000,000(b)
11	QQ09	1448	210	227,170(a)
12	QQ02	1448	210	202,345
13	QQ03	1379	200	1,069,899(a)
14	QQ07	1379	200	742,486(a)
15	QQ08	1379	200	2,820,897
16	QQ05	1310	190	3,641,891(a)
17	QQ10	1310	190	1,386,018(a)
18	QQ01	1310	190	5,000,000(b)
19	QQ04	1379	200	5,000,000(b)
20	QQ06	1448	210	445,268

(a) Nine samples broke in the shoulder, i.e., the grip end with a uniform diameter
(b) Five samples remained intact after 5 million cycles, which was the runout criterion

In most table rows, every sample was inspected for the characteristic and its presence is marked with an "x" and its absence is marked with a blank. However, in a few rows, the authors thought it important to mark "Yes" versus "No" to distinguish between the presence or absence of an attribute, respectively, where every sample was examined. In the final four rows of Table 9 and 10, only a few samples were examined by SEM; in those rows, a blank signifies the sample was not examined, and "Yes" and "No" signify the

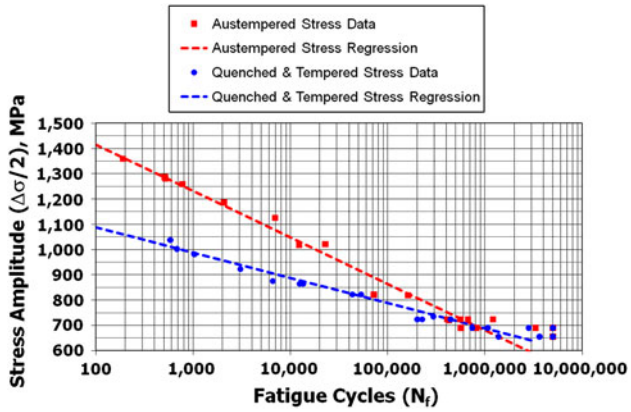

Fig. 11 Semilogarithmic stress amplitude versus fatigue life (for Batches 1 and 2)

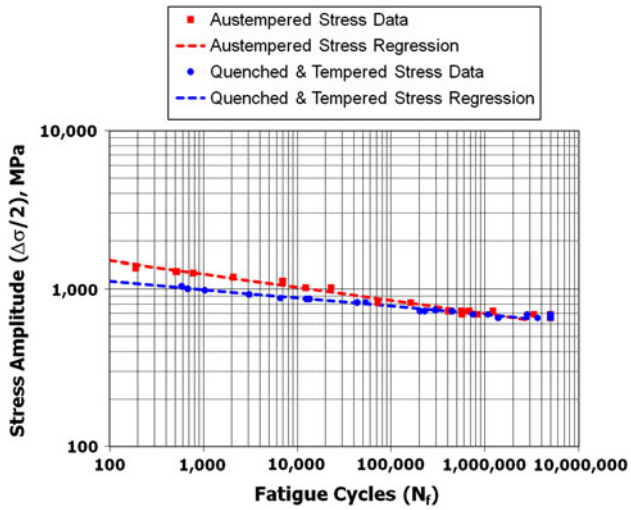

Fig. 12 Logarithmic stress amplitude versus fatigue life (for Batches 1 and 2)

aforementioned absence or presence. Red-colored entries in the table have the most significance.

Typical fractographs of the strain-life fatigue samples are shown in Fig. 14 to 31. There were no significant trends in macroscopic fractographic observations and microscopic fatigue zone fractographic observations with differing strain amplitude, life, or heat treatment type.

All the samples broke in the uniform gage section length of 16 mm, except for one sample (A21); this sample had the highest cycle life in the strain-life fatigue testing. Some of the fatigue cracks nucleated where the extensometer knife edge contacted the sample, as shown in Fig. 14. However, this fact was not considered prejudicial toward causing early failures because multiple fatigue crack initiation sites were found around the circumference of numerous samples, even in the samples where one fatigue crack started at the extensometer blade, as shown in Table 9 and 10. Furthermore, all the sample lives were tightly grouped around the regression curves in Fig. 7 to 9.

Most of the fractures were oriented at 45° to the applied stress axis, and examples are shown in Fig. 14 and 15.

Table 7 Cyclic stress versus life regression constants (Batches 1 and 2)

Condition	Semilogarithmic(a)				Logarithmic(b)			
		Slope, E			Constant, F			
Stress units	Constant, D	MPa	ksi	Coefficient of determination, r^2	MPa	ksi	Slope G	Coefficient of determination, r^2
Austempered	9.7212	−0.0374	−0.0054	0.9768	29.984	40.020	−11.968	0.9750
Q&T	12.862	−0.0100	−0.0691	0.9730	60.003	44.045	−19.032	0.9780

(a) Defining equation: $\log N_f = D + E\,(\Delta\sigma/2)$
(b) Defining equation: $\log N_f = F + G \log(\Delta\sigma/2)$ or $N_f = F\,(\Delta\sigma/2)^G$

Table 8 Staircase fatigue results (Batch 2)

Staircase test result#	Sample ID	Stress amplitude, Δσ/2		Cycles to failure, N_f	Result
		MPa	ksi		
1	AA12	724	105	1,215,605	Fail
2	AA10	689	100	5,000,000	Pass
3	AA13	724	105	672,218	Fail
4	AA06	689	100	3,330,768	Fail
5	AA04	655	95	5,000,000	Pass
1	QQ02	724	105	202,345	Fail
2	QQ08	689	100	2,820,897	Fail
3	QQ01	655	95	5,000,000	Pass
4	QQ09	689	100	5,000,000	Pass
5	QQ06	724	105	445,268	Fail

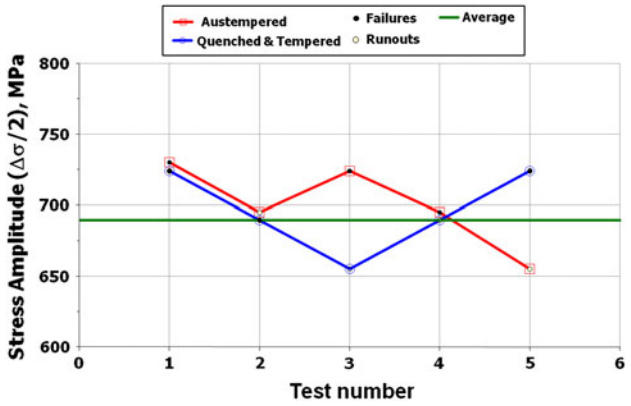

Fig. 13 Staircase stress-life fatigue results for gauge section failures only (for Batch 2). Both austempered and quenched and tempered samples had identical mean fatigue limit of 689 MPa (100 ksi) and standard deviation of 26 MPa (3.8 ksi)

Irrespective of that observation, separate fatigue and overload regions were found in most samples, as shown in Fig. 16 and 17. Ratchet marks and Stage 1 crystallographic cracking were found in multiple samples, as shown in Fig. 16 to 20. However, a thumbnail, Stage 2 fatigue cracking and striations, and a pronounced shear lip were only found in one sample, as shown in Fig. 21 to 24.

Through-cracks were not observed for several samples, as shown in Fig. 17 and 25. Although only a few samples were inspected in the SEM, the microscopic overload characteristics varied significantly between the two heat treatment conditions. Both dimple rupture and quasicleavage were observed for the austempered samples, as shown in Fig. 26 to 28. However, Fig. 29 to 31 shows that dimple rupture was the sole overload fracture morphology observed for the Q&T samples.

4. Discussion

4.1 Comparison of Fatigue Resistance for the Two Heat Treatments

Figure 7 shows that the experimental and predicted total strain versus life behavior were extremely similar for the quench and temper (Q&T) versus the austemper heat treatments. However, the two heat treatments produced opposite effects when the total strain is separated into its elastic and plastic components.

Figure 8 shows that the austempered material has slightly lowers lives at a given *plastic* strain amplitude as compared to the Q&T material. Table 5 shows that the coefficients of determination exceeded 0.9 for the plastic strain regressions, but for lives less than 100, the regression equations predict a greater difference in low cycle fatigue lives than the data points themselves. Therefore, testing at cycles less than 100 may have resulted in convergence in the two datasets and divergence from the Eq 5 log-linear model. Other materials often exhibit lower lives than those predicted by Eq 5.

In contrast, Fig. 9 shows that the austempered material has somewhat higher lives at a given *elastic* strain amplitude. Table 5 and Fig. 10 reflect this behavior in the calculation of the transition fatigue life wherein the Q&T material spent 4.6 times the cycles of austempered material in the plastic strain regime before transitioning to the elastic regime.

The superiority of the austempered material in the elastic strain regime translated into significantly greater high cycle fatigue strengths in the finite life regime near one million cycles, as shown in Fig. 11 and 12. However, Table 6 and Fig. 13 show that identical fatigue limits were obtained for the two heat treatments at 5 million cycles.

Traditional interpretations of these trends suggest that fatigue crack initiation takes significantly longer lives to initiate for the austempered material, although cracks in the Q&T material propagate slightly slower. It should be noted that Fig. 4 shows that there is some untempered martensite in the austempered bainite. It was beyond the scope of this study to determine the effect of untempered martensite on the properties and fracture behavior of austempered bainite.

Table 9 Fractographic observation summary for austempered strain-life fatigue samples

Test Parameters & Observations:	Test Order:	1	2	3	4	5	6	7	8	9	10	11
Specimen ID		A1	A2	A4	A19	A9	A16	A17	A21	AU1	AU2	AU3
Strain Amplitude, Δε/2 (%)		0.5	0.5	1	1.4	0.75	0.6	0.4	0.35	0.4	1.2	1
Cycles, N_f		22,886	12,275	772	189	2,073	6,954	72,017	429,013	162,044	510	517
Through-Crack		No	No	No	Yes	No	No	Yes	Yes	No	No	Yes
Initiation at Extensometer		No	No	Yes	Yes	Yes	No	No	No	No	No	Yes
Multiple Secondary Cracks					x							
Multiple Initiation Sites		x			x				x			
Ratchet Marks		x							x			x
Beach Marks												
Thumbnails								x				
Discrete Fatigue & Overload Zones		x		x	x			x	x			x
Shear Lip		x						x				x
Oriented 45-degrees				x	x	x	x		x	x	x	x
Stage 1 (crystallographic) fatigue cracking				x								x
Rub marks		x		x								
Shear or Tear												
Striations & Stage 2 (noncrystallographic) Striation Cracking								x				
Inclusions & Woody Fracture				x								
Dimple Rupture		Yes		Yes				Yes				
Quasicleavage		Yes						Yes				

Table 10 Fractographic observation summary for quenched and tempered (Q&T) strain-life samples

Test Parameters & Observations:	Test Order:	1	2	3	4	5	6	7	8	9	10
Specimen ID		Q9	Q15	Q19	Q17	Q18	Q16	Q20	Q21	QU1	QU2
Strain Amplitude, Δε/2 (%)		0.5	0.5	1	1	1.2	0.6	0.4	0.35	0.75	0.4
Cycles, N_f		13,479	12,408	681	1,029	583	6,575	43,319	294,680	3,066	53,503
Through-Crack		Yes	No	Yes	Yes	Yes	No	Yes	Yes	Yes	Yes
Initiation at Extensometer		No	No	No	Yes	Yes	Yes	No	No	No	No
Multiple Secondary Cracks		x									
Multiple Initiation Sites		x			x				x	x	x
Ratchet Marks		x				x				x	
Beach Marks		x			x						
Thumbnails											
Discrete Fatigue & Overload Zones		x		x		x		x	x	x	x
Shear Lip						x					
Oriented 45-degrees		x		x	x	x	x	x	x	x	x
Stage 1 (crystallographic) fatigue cracking		x				x					
Rub marks		x			x						
Shear or Tear		?			?						
Striations & Stage 2 (noncrystallographic) Striation Cracking											
Inclusions & Woody Fracture					x						
Dimple Rupture		Yes			Yes						
Quasicleavage		No!			No!						

Even if the reader remains unconvinced about the fatigue resistance differences between the two materials, it is still noteworthy that the two heat treatments produce similar fatigue properties at the same levels of hardness and monotonic strength. Without reaching any truly definitive distinction, this study represents another contribution to the differing results obtained by earlier investigators (Ref 6-12) as they investigated the microstructural effects on strain-life and stress-life properties of martensitic steel formed Q&T heat treatment versus bainitic steel formed by isothermal austempering heat treatment.

4.2 Comparison of Fractographic Characteristics for the Two Heat Treatments

Both heat treatments produced similar fatigue fracture morphologies. The largest notable observation is that both the austempered and the Q&T samples were notch sensitive, which resulted in shoulder fractures in the high cycle regime from 400,000 to 5 million cycles. Note that there was only one shoulder break (sample A21) obtained in the strain-life testing (see Table 4), whereas multiple shoulder fractures were obtained in the stress-life failures (see Table 6). The greater shoulder radius and generally lower testing loads for the stress-life samples (see Fig. 2) versus the strain-life samples (see Fig. 1) were insufficient to reduce the stress concentration and avoid shoulder breaks.

In their earlier study (Ref 3), the authors investigated fracture surfaces of Charpy V-notch test samples tested between 0 C (32 F) to 100 C (212 F), as well as the fracture surfaces of slow bend specimens tested at room temperature at a low crosshead speed 0.025 mm/min (0.001 in./min). Charpy V-notch tests are conducted at a velocity of 4.5 m/s or 270,000 mm/min (Ref 38). At most test temperatures, both

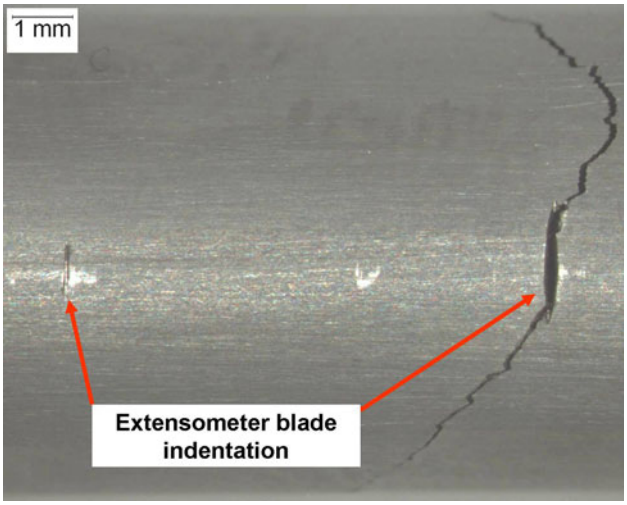

Fig. 14 Optical (stereoscopic) image in profile of fatigue crack nucleation at the right-hand extensometer blade witness mark in sample A4 tested at a strain amplitude (ε_a) of 1% with cycles to failure (N_f) of 772. Note the 45° angle profile of the fatigue crack, and its stage 1 (mountainous and crystallographic) character. Original magnification (OM) = 10×

Fig. 15 Optical image of 45° fatigue crack orientation in profile view of sample Q17 tested at a ε_a of 1% with N_f of 1,029

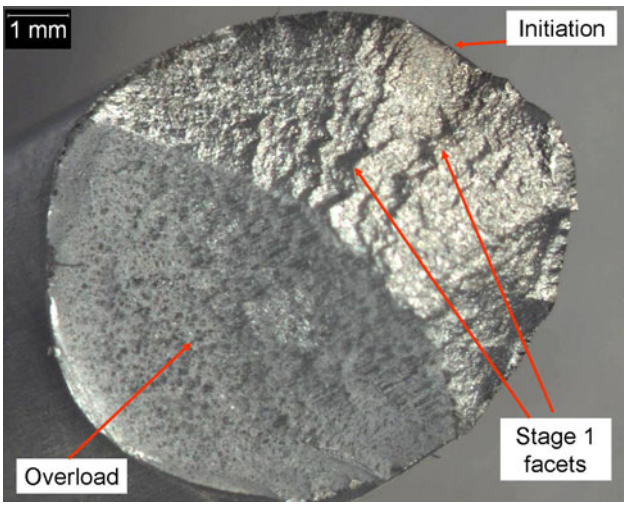

Fig. 16 Optical image of fatigue crack initiation at extensometer witness mark, Stage 1 crystallographic fatigue cracking, and separate fatigue and overload regions in sample A4 tested at a ε_a of 1% with N_f of 772. OM = 10×

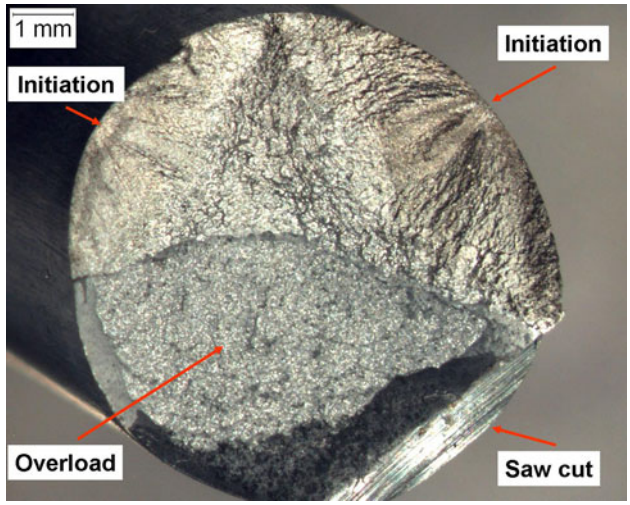

Fig. 17 Optical image multiple fatigue crack initiation sites, separate fatigue, and overload regions, and saw cut used to finish the crack in sample A1 tested at a ε_a of 0.5% with N_f of 22,886. OM = 10×

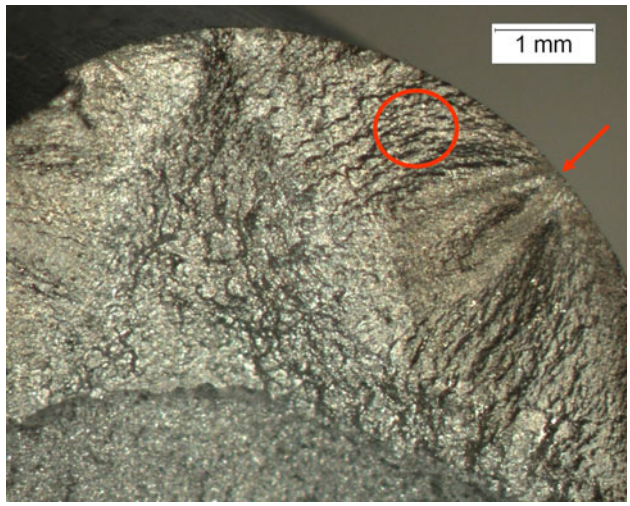

Fig. 18 Higher-magnification view of Fig. 17 showing one of the fatigue crack nucleation sites (see arrow) and Stage 1 crystallographic cracking (circled) in sample A1 tested at a ε_a of 0.5 % with N_f of 22,886. OM = 16×

the austempered and the Q&T steels Charpy and bend samples exhibited similar mixed fracture morphologies of quasicleavage and dimple rupture although the Q&T steel exhibited less dimple rupture.

Using the nominal gauge length of 16 mm shown in Fig. 2, and the fatigue strain rate of 2%/s, the overload zones of the strain-life samples were tested in this study at a crosshead speed of approximately 1,920 mm/min (76 in./min). It is noteworthy that the austempered strain-life samples from this study exhibited similar overload fracture morphology to the Charpy and bend samples from the previous study (Ref 3). However, the Q&T strain-life samples exhibited no quasicleavage and only dimple rupture in this study.

Faster testing rates would tend to promote less dimple rupture, and the strain-life overload speed is intermediate

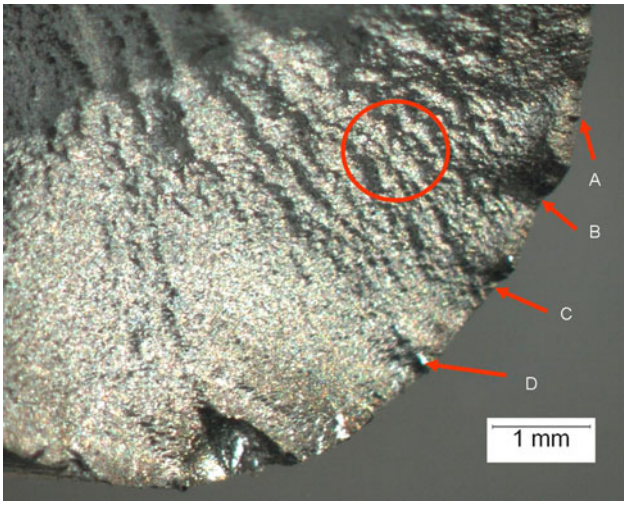

Fig. 19 Optical image of multiple fatigue crack nucleation sites and ratchet marks (see arrow), and Stage 1 crystallographic cracking (circled) in sample Q9 tested at a ε_a of 0.5% with N_f of 13,479. OM = 16×

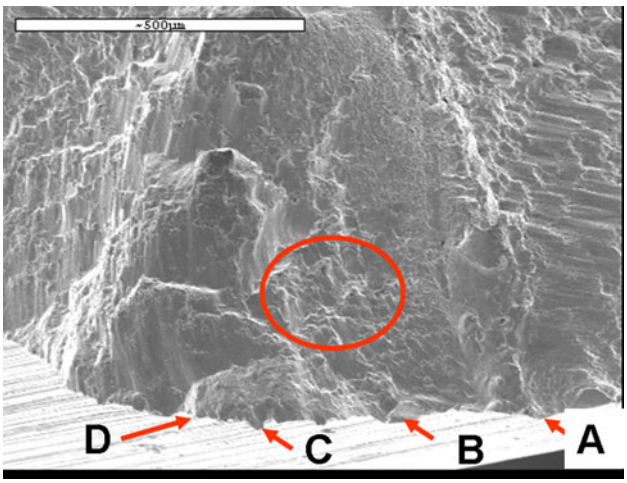

Fig. 20 Corresponding secondary electron (SE) image to Fig. 19 of sample Q9 tested at a ε_a of 0.5 % with N_f of 13,479. The arrows, circles, and letters represent the same features in Fig. 19, after rotation about 45° clockwise. OM = 100×

between the very fast Charpy and very slow bend test rate. Furthermore, the earlier study showed that the Q&T samples had less tendency toward dimple rupture than the austempered samples. The dimple rupture tendency for overload in the Q&T strain-life samples is thus unexplainable on face value; however, it may be that the cementite particle and dislocation deformation substructure established by cyclic strain-life fatigue testing caused the different overload fracture morphology behaviors for the Q&T samples.

5. Conclusions

In room temperature and fully reversed fatigue testing of austempered versus quenched and tempered (Q&T) 4340 steel

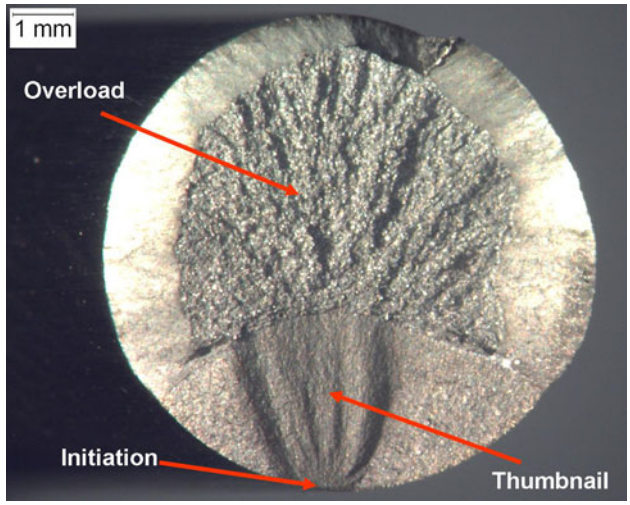

Fig. 21 Fatigue initiation site, thumbnail, and overload zone in optical image of sample A17 tested at a ε_a of 0.4% with N_f of 72,017. OM = 10×

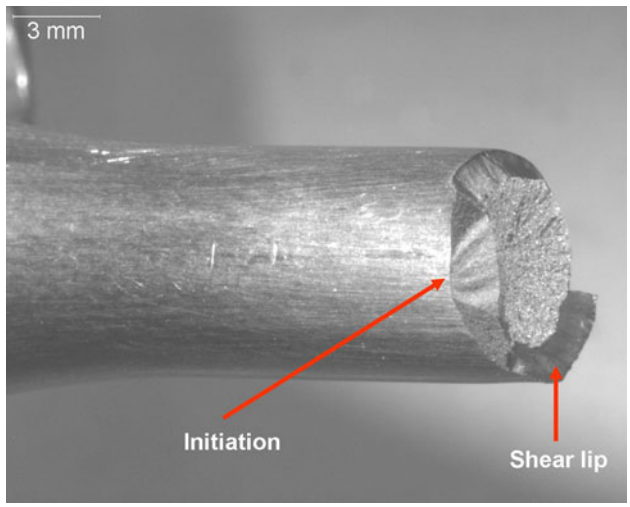

Fig. 22 Optical image in profile of initiation site (see Fig. 21) and shear lip in sample A17 tested at a ε_a of 0.4% with N_f of 72,017. OM = 4.8×

samples that were heat treated to the same hardness and monotonic strength, the following results were obtained:

1. The two heat treatments produced virtually identical total strain-life curves and fatigue limits at 5 million cycles.
2. The austempered steel had greater high cycle fatigue lives than the Q&T samples at constant elastic strain and stress amplitudes.
3. Austempered steel had marginally lower lives at constant plastic strain amplitude versus the Q&T samples.
4. The mixed fatigue behavior is consistent with the differences observed by other authors.
5. Fractographic characterization showed that both heat treatments produced notch sensitive behavior and similar fatigue cracking morphology. However, the overload fracture morphology in the strain-life test samples tested at

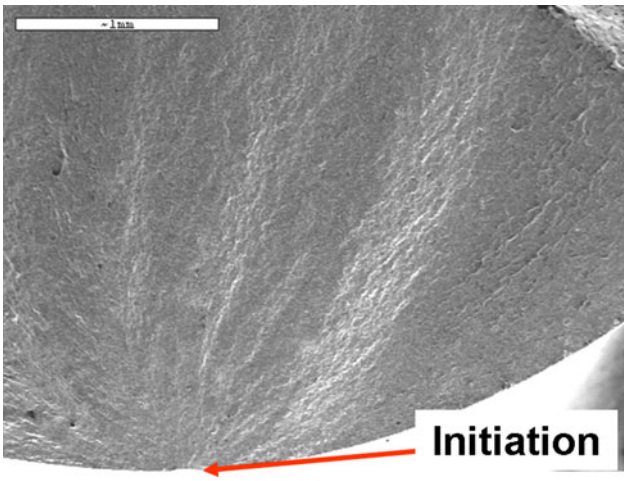

Fig. 23 SE image of initiation site in sample A17 tested at a ε_a of 0.4% with N_f of 72,017. The equivalent optical view is shown in Fig. 22. OM = 35×

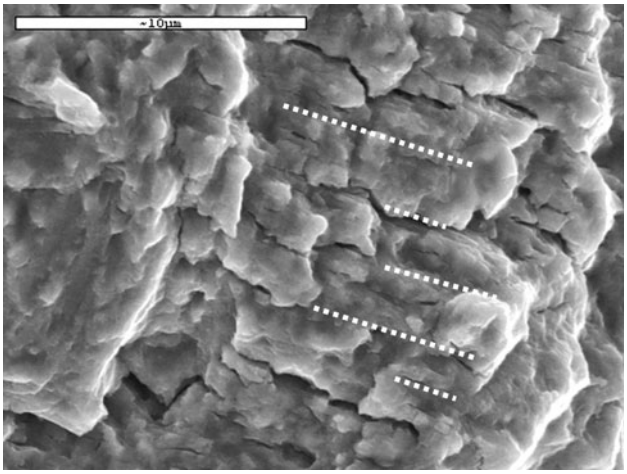

Fig. 24 SE image of striations and striation cracking marked by dashed lines in sample A17 tested at a ε_a of 0.4 % with N_f of 72,017. OM = 5000×

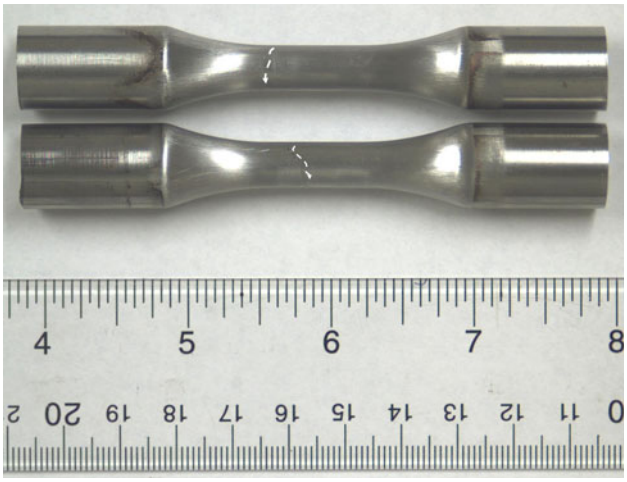

Fig. 25 Optical image of partial crack progression in direction of dashed arrows for samples A1 (top) and A4 (bottom) tested at a ε_a of 0.5 and 1% with N_f of 22,886 and 772

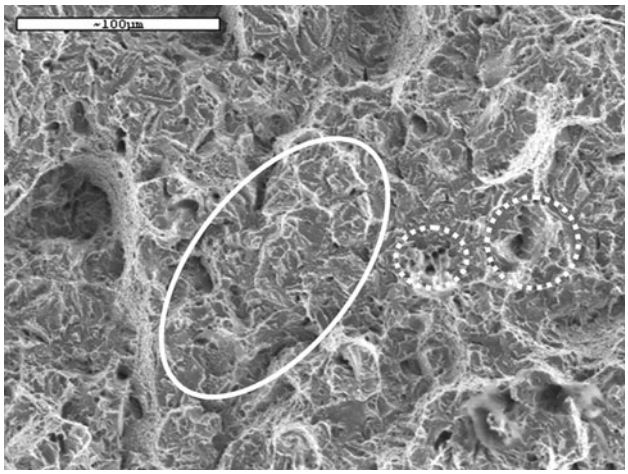

Fig. 26 SE image of quasicleavage within solid ellipse and dimple rupture within dashed circles in sample A1 tested at a ε_a of 0.5% with N_f of 22,886. OM = 350×

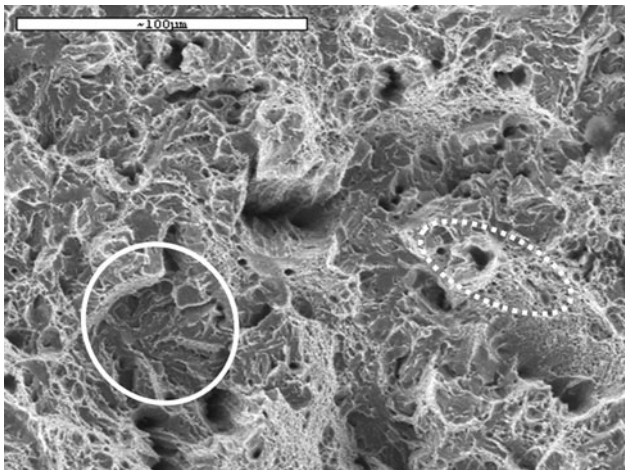

Fig. 27 SE image of quasicleavage within solid ellipse and dimple rupture within dashed ellipse in sample A17 tested at a ε_a of 0.4% with N_f of 72,017. OM = 350×

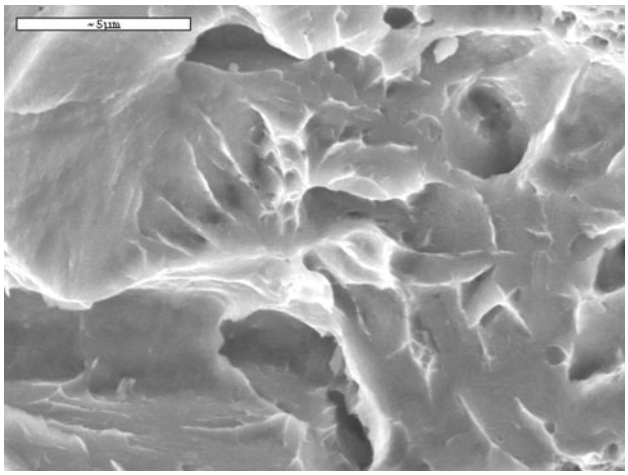

Fig. 28 SE image of quasicleavage in single grain of sample A17 tested at a ε_a of 0.4% with N_f of 72,017. OM = 6000×

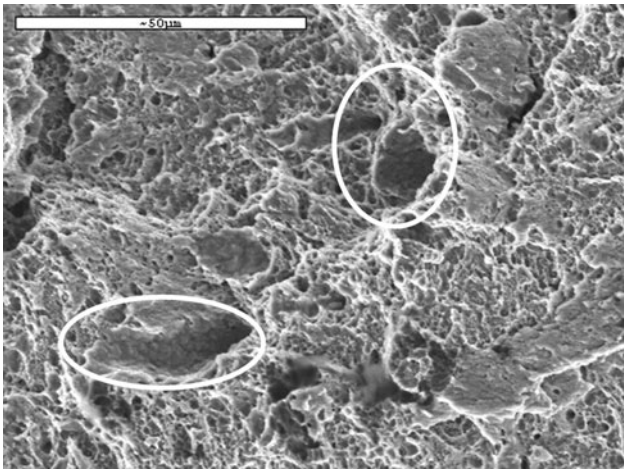

Fig. 29 SE image of dimple rupture throughout sample Q17 tested at a ε_a of 1% with N_f of 1,029. The small dimples were probably nucleated by small cementite particles, and the large dimples (within ellipses) are associated with nonmetallic inclusions. OM = 1000×

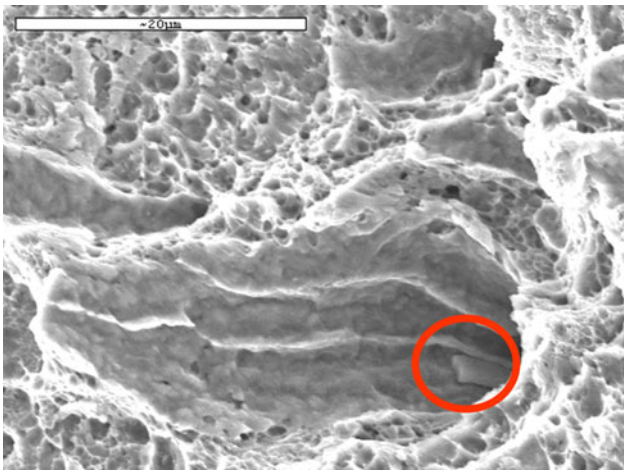

Fig. 30 Higher-magnification SE image of dimple rupture throughout sample Q17 tested at a ε_a of 1% with N_f of 1,029. The circled feature is a MnS stringer inclusion remnant. OM = 2500×

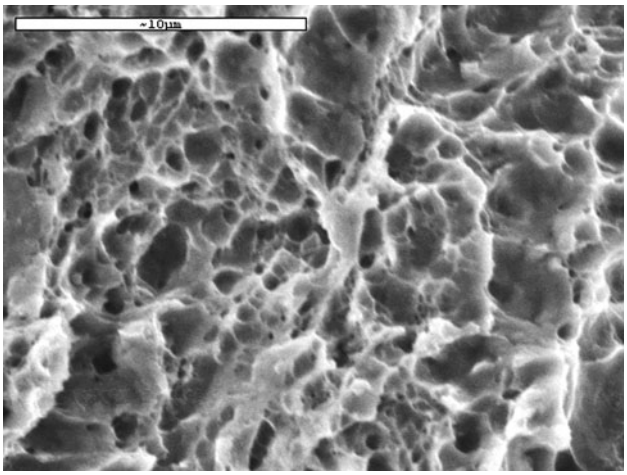

Fig. 31 High-magnification SE image of dimple rupture throughout sample Q9 tested at a ε_a of 0.5% with N_f of 13,479. OM = 5000×

intermediate strain rates was slightly different between the heat treatments, which contrasted with the authors' earlier study that showed similar overload fracture morphologies over a wide range of strain rates.

Acknowledgements

The authors thank all the test technicians at Stork Climax Research Services (CRS) and Terry Lusk at Applied Process, Inc. for meticulously conducting the experiments.

Appendix

Strain-Reversals and Strain Hardening Fatigue Equations and Symbols

The total strain amplitude ($\Delta\varepsilon/2$) was the controlled variable in the fatigue tests. The total strain amplitude was equated to the sum of its elastic ($\Delta\varepsilon_e/2$) and plastic ($\Delta\varepsilon_p/2$) components, i.e.,

$$(\Delta\varepsilon/2) = \Delta\varepsilon_e/2 + \Delta\varepsilon_p/2 \quad \text{(Eq 1)}$$

The elastic strain amplitude was calculated using Hooke's Law (E = Young's or elastic modulus) and the saturation stress amplitude ($\Delta\sigma/2$) obtained at half-life (0.5 N_f) as follows:

$$\Delta\varepsilon e/2 = \Delta\sigma/2E \quad \text{(Eq 2)}$$

The plastic strain amplitude ($\Delta\varepsilon_p/2$) was calculated by subtraction, i.e.,

$$\Delta\varepsilon_p/2 = \Delta\varepsilon/2 - \Delta\varepsilon_e/2 = \Delta\varepsilon/2 - \Delta\sigma/2E \quad \text{(Eq 3)}$$

The saturation stress ($\Delta\sigma/2$) and the plastic strain ($\Delta\varepsilon_p/2$) amplitudes were related to the number of reversals ($2N_f$)

$$\Delta\sigma/2 = \sigma'_f\,(2N_f)^b \quad \text{(Eq 4)}$$

and

$$\Delta\varepsilon_p/2 = \varepsilon'_f(2N_f)^c \quad \text{(Eq 5)}$$

where the four constants σ'_f, b, ε'_f, and c are the fatigue strength coefficient, fatigue strength exponent, fatigue ductility coefficient, and the fatigue ductility exponent, respectively, determined using linear regression. The above equations were combined to obtain the overall total strain amplitude-life equation.

$$\Delta\varepsilon/2 = \left(\sigma'_f/E\right)(2N_f)^b + \varepsilon'_f(2N_f)^c \quad \text{(Eq 6)}$$

The monotonic (Ref 3) and cyclic stress-plastic strain behavior of the steels was characterized using the equation

$$\sigma = K\varepsilon_p^n \quad \text{(Eq 7)}$$

and

$$\Delta\sigma/2 = K'\left(\Delta\varepsilon_p/2\right)^{n'} \quad \text{(Eq 8)}$$

where K is the monotonic strength coefficient, n is the monotonic strain hardening exponent, σ is the true tensile stress, ε_p is the true plastic tensile strain, K' is the cyclic strength coefficient, and n' is the cyclic strain hardening exponent. The

four constants (K, n, K', and n') were determined using linear regression. A material is considered as cyclically softening when the cyclic stress amplitude is lower than the monotonic true stress, i.e. $\Delta\sigma/2 < \sigma$, for a given plastic strain; cyclic hardening is the opposite situation.

The above Eq 4, 5, 7, and 8 in the form of $y = Ax^B$ were transformed to $\log y = \log A + B \log x$ for the purposes of obtaining the linear regression constants A and B. As is common practice in ASTM standards E606 (Ref 26) and E739 (Ref 30), the fatigue reversals regression analyses for Eq 4 and 5 were performed with the equations inverted, i.e., with fatigue reversals as the dependent variable and the stress or strain amplitude as the independent variable, which is the opposite of how fatigue data is usually plotted.

The transition fatigue life (N_t) can be obtained by equating the two terms on the right-hand side of Eq 6. The defining equation is as follows:

$$N_t = 0.5\left(\varepsilon'_f E/\sigma'_f\right)^{1/(b-c)} \quad \text{(Eq 9)}$$

Stress-Life Fatigue Equations and Symbols

In stress-life fatigue testing, the life is often related to the stress by the semilogarithmic equation:

$$\log N_f = D + E\,(\Delta\sigma/2) \quad \text{(Eq 10)}$$

or in its logarithmic form:

$$\log N_f = F + G\log(\Delta\sigma/2) \quad \text{(Eq 11)}$$

which converts to the equation

$$N_f = F\,(\Delta\sigma/2)^G \quad \text{(Eq 12)}$$

As with the reversals equations, the stress-life regression analyses for Eq 10 and 11 were performed with the equations inverted as is common practice in ASTM standard E739 (Ref 30).

References

1. K. Brandenberg, K. Hayrynen, and J.R. Keough, Austempered Gears and Shafts: Tough Solutions, *Gear Technol.*, 2001, **18**(2), p 42–50
2. ASM Handbook: *Properties and Selection: Irons, Steels, and High-Performance Alloys. Notch Toughness of Steels*, 10th Ed., Vol. 1, ASM International, Materials Park, OH, 1990, p 748, which cites the original paper: R.F. Hehemann, V.J. Luhan, and A.R. Troiano: "The Influence of Bainite on Mechanical Properties," *Transactions of American Society for Metals (ASM)*, Vol. 49, 1957, p 409–426
3. J.M. Tartaglia, K.A. Lazzari, G.P. Hui, and K.L. Hayrynen, A Comparison of Mechanical Properties and Hydrogen Embrittlement Resistance of Austempered versus Quenched & Tempered 4340 Steel, *Metall. Mater. Trans.*, 2008, **39A**(3), p 559–576
4. L.F. Reynolds and M.P. Hayes, Factors Affecting Delayed Failure in Electroplated Carbon Spring Steels, *Trans. Inst. Met. Finish*, 1987, **65**(2), p 50–57
5. J.-R. Hwang, K.-P. Peng, and C.-C. Wang, Effect of Second Phase on the Fatigue Crack Growth in AISI, 4340 Steel, *J. Mater. Sci. Lett.*, 1996, **15**(3), p 192–196
6. Y. Tomita, F. Kijima, and K. Morioka, Modified Austempering Effect on Bending Fatigue Properties of Fe-0.6C-1.5Si-0.8Mn Ateel, *Mater. Res. Adv. Tech.*, 2000, **91**(1), p 43–46 (in German)
7. H. Hengerer, Raising the Fatigue Strength of High-Duty Steels by Austempering, *Sulzer Tech. Rev.*, 1969, **51**(2), p 72–79
8. L. Ban, W. Hui, Q. Yong, Y. Weng, and H. Dong, High Cycle Fatigue Behavior of Medium-Carbon Trip Steel at Different Tensile Strength Levels, *Chin. J. Mater. Res.*, 2008, **22**(6), p 629–633 (in Chinese)
9. S. Zheng, B. Tian, L. Wu, and Q. Dong, Influence of Tempering Temperature on the Properties of B/M Duplex Structure in Steel LM-2, *Heat Treat. Met.*, 1993, **2**, p 3–8 (in Chinese)
10. P. Raviazz and C. Giometto, Fatigue Behavior of Structural Steels After Quenching and Tempering or After Bainitic Quenching (Austempering), *Rev. Met.*, 1970, **67**(6), p 531–538
11. M.T. Yu, T.H. Topper, and L. Wang, Effect of Microstructure on the Mechanical Behaviour of a Low Carbon, Low Alloy Steel, *Int. J. Fatigue*, 1988, **10**(4), p 249–255
12. J.M. Tartaglia, The Effects of Martensite Content on the Mechanical Properties of Quenched and Tempered 0.2%C-Ni-Cr-Mo Steels, *J. Mater. Eng. Perform.*, 2010, **19**, p 572–584, online: July 15, 2009, http://dx.doi.org/10.1007/s11665-009-9503-x
13. Y. Li, Fatigue Fracture Behavior of Low Carbon Martensite and Martensite/Bainite Duplex Structure in Steel, *Phys. Metall. Mater. Sci.*, 1992, **5A**(3), p 212–217 (in Chinese)
14. S.M. Safi and M.K. Besharati, A New Modified Austempering to Increase Strength and Ductility Simultaneously for UHS Steels, Defect and Diffusion Forum in Diffusion in Solids and Liquids, 2010, **297–301**, p 1109–1115
15. SAE Information Report J1099, Technical Report on Low Cycle Fatigue Properties: Ferrous and Nonferrous Steels, SAE, Warrendale, PA, August 2002
16. M. Ogasawara, Crack Initiation at Notches in Low Cycle Fatigue, *Mechanical Behavior of Materials, Symposium Proceedings*, August 21–23, 1973, Kyoto, Japan, 1974, p 159–176
17. D.L. Turner, F.J. Worzala, Austempered Steel Mower Blades—The Effect of Heat Treatment on Structure and Properties, *Proceedings of International Symposium for Testing and Failure Analysis (ISFTA)*, 1985, p 352–356
18. American Iron and Steel Institute's Bar Steel Fatigue Database, http://www.autosteel.org/AM/Template.cfm?Section=Steel_Bar_and_Rod1
19. Surface Chemical Analysis—Glow Discharge Optical Emission Spectrometry (GD-OES)—Introduction to Use, ISO14707:2000E, First Edition (2000-18-15), ISO
20. "Standard Test Methods for Determination of Carbon, Sulfur, Nitrogen, and Oxygen in Steel, Iron, Nickel, and Cobalt Alloys by Various Combustion and Fusion Techniques," E1019-08, ASTM International
21. "Standard Test Methods for Rockwell Hardness of Metallic Materials," E18-08b, ASTM International
22. "Standard Guide for Preparation of Metallographic Specimens," E3-01 (2007)ε1, ASTM International
23. "Standard Test Methods for Tension Testing of Metallic Materials1," E8/E8M-09, ASTM International
24. "Standard Test Method for Young's Modulus, Tangent Modulus, and Chord Modulus," E111-07, ASTM International
25. "Standard Test Method for Tensile Strain-Hardening Exponents (n-Values) of Metallic Sheet Materials1," E646-07, ASTM International
26. "Standard Practice for Strain-Controlled Fatigue Testing," E606-04ε1, ASTM International
27. "Standard Practice for Stress-Controlled Fatigue Testing," E466-07, ASTM International
28. "Standard Terminology Relating to Fatigue and Fracture Testing, E1820, ASTM International
29. W.J. Dixon and A.M. Mood, A Method for Obtaining and Analyzing Sensitivity Data, *J. Am. Stat. Assoc.*, 1948, **43**, p 109–126
30. "Standard Practice for Statistical Analysis of Linear or Linearized Stress-Life (S-N) and Strain-Life (e-N) Fatigue Data," E739-91(2004)ε1, ASTM International
31. R.E. Little, *Manual on Statistical planning and Analysis*, ASTM Standard Technical Publication (STP), Materials Park, 1975, p 54ff
32. J. Song, P.N. Crepeau, Z.P. Mourelatos, R.J. Gu, Sensitivity Study of Staircase Fatigue Tests Using Monte Carlo Simulation, Paper No. 2005-01-0803, SAE International, 2005
33. "Specification and Verification of Tensile and Fatigue Properties in Cast Components," GMN7152, GM Engineering Standard, February 2002
34. "Chemical Compositions of SAE Alloy Steels," J404, JUN2000, SAE International

35. "Steel, Bars, Forgings, and Tubing 0.80Cr-1.8Ni-0.25Mo (0.38-0.43C) (SAE 4340)," AMS-6415R, June 2003, SAE International
36. "Standard Test Methods and Definitions for Mechanical Testing of Steel Products," A370-09aε1, ASTM International
37. J.A. Bannantine, J.J. Comer, and J.L. Handrock, *Fundamentals of Metal Fatigue Analysis*, Prentice-Hall, Upper Saddle River, NJ, 1990, p 61
38. "Standard Test Methods for Notched Bar Impact Testing of Metallic Materials," E23-07aε1, ASTM International